Measurement of the step size of the molecular motor, *dynein*

Patrick N. Lawlor
Advisor: George Shubeita, PhD

Signature _____

Department of Physics
University of Texas at Austin

May 7, 2010

Contents

List of Figures

List of Tables

1 Introduction

At any given time, an enormous number of different events are occurring in every living cell - that cells function predictably and reliably is a testament to nature's superb engineering. One of the most vital components of the cell that aids in the organization and coordination of this hodgepodge is a protein called the molecular motor. Like a man-made motor, the molecular motor converts chemical energy into useful mechanical work (some types even function in reverse). The type of molecular motor that is the subject of this work is called the 'microtubule-based transport molecular motor', the type responsible for shuttling various types cargos around the cell. Many important cargos - vesicles, organelles, large nucleic acid sequences - are far too large to diffuse to their targets within the cell on a biologically relevant timescale. Cells divide on the scale of minutes; hours, days, or years can pass before large types of cargo would reliably diffuse along the length of some types of cells (e.g., meter-long nerve cells).

Because molecular motors provide such an important and pervasive mechanism of transport, their malfunctions have the potential to deleteriously affect the function of an organism to a high degree. Most human diseases whose causes have been linked to molecular motor malfunction or deficiency are neurological in nature. Molecular motors have been implicated in neurodegenerative diseases such as Huntington's and Alzheimer's diseases, and developmental diseases such as lissencephaly (the condition of the brain lacking folds) [21]. Understanding their function is not only an issue of basic science, but one of medical relevance.

1.1 Background on proteins

Like all other proteins, the molecular motor is the end product of a process common to all living organisms, the 'central dogma'. Information about how to construct a particular component (e.g., a molecular motor) of an organism is encoded as a sequence of 'bits' (subunits) in a DNA polymer as a gene. A single molecule of DNA contains many genes. When conditions are such that an organism needs to produce a certain one of its components, a copy of the gene that encodes that component is produced using RNA - very similar to DNA but with a minor chemical difference. A cellular machine called the ribosome translates the RNA copy of a gene into yet another polymer: a sequence of amino acids (a protein). There are 20 naturally occurring amino acids, all with the same basic structure except for one functional group. Some functional groups are acidic, some basic, some charged, some neutral, and some polar. It is these differences that are responsible for how different amino acids interact with each other, and ultimately, how an amino acid polymer folds into a stable conformation. Proteins may, however, have more than one stable conformation; the molecular motor is one such example of a dynamic protein. It could not produce mechanical work if it could not alternate between at least two conformations. The detailed mechanism of motion will be discussed later.

1.2 The motors - *kinesin* and *dynein*

1.2.1 Similarities

Microtubule-based molecular motors constitute only one class of molecular motor proteins, and even within this class there are multiple types of motors. This work

focuses on two: kinesin and, to a greater extent, dynein. The two proteins share many functional features despite distinct structural composition. Both motors are approximately 100 nanometers in their longest dimension [20]. Both motors extract energy from the same chemical fuel, adenosine triphosphate (ATP), by hydrolysis of one of its phosphate groups. This typically yields approximately 50 kJ/mol under cellular conditions and occurs in a part of the protein called the motor domain. Both motors transport the same types of cellular cargo: cell organelles (mitochondria, golgi bodies), vesicles (synaptic and otherwise), and RNA [Hirokawa, Nature Rev 2009]. Often, both types of motors attach to a particular cargo simultaneously - the implications of this are extremely important and will be discussed later.

The most important similarity, however, is that both motors locomote in the same fashion. Both have rudimentary legs (actually called heads) and 'walk' like bipeds along protein polymers called microtubules [4] (figure 1) - hence 'microtubule-based molecular motor'. Cells synthesize the protein subunits of microtubules, tubulin, and polymerize them into chains as long as a few micrometers. Both types of motors' heads have very specific binding sites that allow them to attach to tubulin subunits (subunit spacing is approximately 8 nm). Tubulin subunits [figure] are asymmetrical and polymerize preferentially in one orientation; this ultimately gives rise to global polarity, with each microtubule having a so-called plus-end and minus-end [12]. This polarity will also be very important to the movement of the molecular motors and will be discussed at length.

Roughly speaking, the mechanism of converting the energy of ATP to mechanical work is similar between the two motors, although the details are neither exactly the

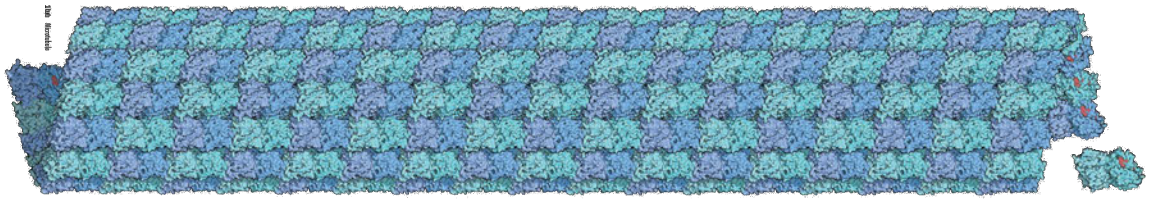

Figure 1: Molecular motors walk on microtubules, cytoskeletal filaments composed of tubulin dimer subunits.

same nor agreed upon for each motor. First, ATP diffuses to its binding site on the head bound to the microtubule and binds. This causes a conformational change in the head; ATP binding cocks the leg into a high energy conformation that pulls the other, non-attached head forward in a step motion so that it binds to a tubulin subunit ahead of the first head. The first head now hydrolyzes its ATP into ADP and an inorganic phosphate. This process repeats for the head now in front. This is called the hand-over-hand model of stepping. The nature of the conformational changes that hurl one head in front of the other are the details that are not well understood [24].

1.2.2 Kinesin Overview

Even though there are many variants within kinesin family - mammals alone have 45 different types of kinesin [hirokawa, nature rev 2009] - they all share a very similar structure. Most types of kinesin are tetramers comprised of two types (two of each)

of proteins: a 'heavy chain' which contains the motor domain (the motor itself), and a 'light chain' which connects the motor domain to the cargo. Kinesin is typically approximately X nm in length and weighs approximately X kDa. Each motor domain of a kinesin has one binding site for ATP, the motor's chemical fuel. Very importantly, most types of kinesin walk only towards the plus-ends of mictrotubules (kinesin-1 and kinesin-2, important to this study, walk only towards the plus-end).

Figure 2: The molecular motor, *kinesin*

1.2.3 Dynein Overview

There exists only one type of dynein transport motor - called cytoplasmic dynein - across nearly all species [20], and it is a significantly more complicated motor than kinesin. While kinesin is composed of only four protein chains, dynein is composed of twelve: two heavy chains which contain the motor domains (like kinesin), six

intermediate-weight chains, four light chains. Dynein is typically X nm in length, and due to the large number of protein chains, weighs approximately 1.5 MDa. Dynein walks only towards the minus-ends of microtubules.

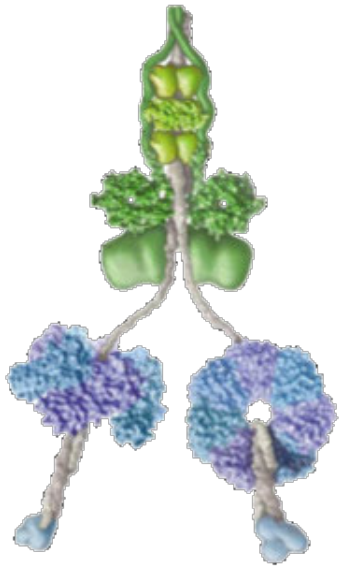

Figure 3: The molecular motor, *dynein*

1.3 Why are molecular motors interesting to physicists?

The physics community has participated in the study of molecular motors since their discovery, and continues to do for a number of reasons. The molecular motor represents one of the smallest, if not the smallest, examples of a naturally occurring motor, and one of amazing efficiency. In contrast to the average internal combustion engine with average efficiency of approximately 20%, kinesin achieves an efficiency of nearly 50%.

In addition, studying the dynamical behavior of single molecules basically requires

the use of precise tools that physics can offer. Measuring the bulk properties of molecular motors offers little information about single molecule dynamics because of the lack of synchronization between motors. That is, understanding the net behavior of all of the motors in a single cell can tell you little about the intra-molecular behavior of a molecule whose distinguishing feature is its richness as a single unit.

A great deal of the important work done to understand molecular motors has made use of both experimental and theoretical/computational physical tools. Powerful types of microscopy such as Differential Interference Microscopy (DIC) have allowed us to visualize motor function in real time. X-ray crystallography has allowed us to solve the three-dimensional structures of some important parts of different molecular motors. Theoretical and computational tools have allowed us to develop models that generate predictions that can be experimentally tested. Optical tweezers have allowed us to exert forces on single motors and to track motor position with extremely high temporal and spatial precision. Examples of work that used optical tweezers can be found below.

1.4 Important Contemporary Work

A great deal has been learned about the function of molecular motors during the past few decades. This section will serve to summarize some of the most important results and techniques.

1.4.1 Motor structure

Besides the discovery of the motor proteins and their functions as transporters, some of the most important initial work involved understanding their three dimensional structures. The first attempts made at revealing the structures of the motors involved electron microscopy. In 1985, Vale and Amos (independently) were the first to visualize kinesin purified from the brains of the squid and pig respectively (figure 4). Amos wrote that kinesin "appears to consist of a fine rod with a large disordered domain at one end and a smaller domain at the other." - very rudimentary. Based upon these micrographs, they estimated the approximate size of kinesin to be between 50-120 nanometers.

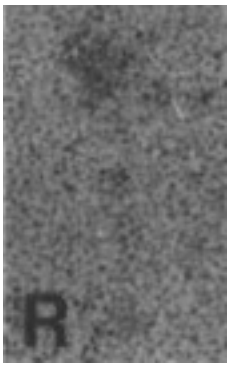

Figure 4: Early electron micrograph of *kinesin*

Using x-ray crystallography, Vale was the first to solve the structure of the motor domain of kinesin-1 in 1996 [Vale, 1996, Nature], providing us with the first high-precision map. In addition to more detailed properties, he discovered the location of the ATP binding site on the surface of the motor domain as well as the location at which the motor domain attaches to the microtubule. Since then, crystal structures

of different variations and conformations of kinesin have been published.

Being much larger and more complicated, dynein's motor domain has not been crystallized yet. Some of the smaller proteins that constitute dynein - two different 'light' chains [Hendrickson][Liang] - have been crystallized, but they shed no light on the core of the motor itself. Despite this, electron microscopy has revealed that dynein is, in fact, a much more complicated motor than kinesin. King discovered that within the dynein motor domain's DNA, there were six ATP hydrolysis sites coded for, as opposed to kinesin's one site. He confirmed this with electron microscopy [King, J Cell Sci, 2000]. Although more recent work shows that not all of the binding sites can hydrolyze ATP, this finding begs questions about the utility of multiple ATP binding sites which have still not been answered.

1.4.2 Motor Function

Measuring the properties of these motors' function and understanding how and why they behave way they do have been the most significant and important challenges of the field. Function spans questions from the mechanics of stepping to how multiple motors coordinate to move a single cargo. Scientists using physical tools have again contributed enormously to this field.

In addition to revealing some features of the motors' structure, early electron microscopy studies - micrographs taken of cellular cargos that were attached to microtubules - hinted at the fact that multiple motors may attach to a single cargo in living organisms, complicating our picture of cellular transport [Lasek, 1985, J Cell Bio]. EM could not distinguish between different types of motors, and so it was

unclear whether or not the motors were entirely of one type.

Because the living cellular environment is a difficult environment in which to perform controlled experiments, many investigators turned to in vitro experiments - those done on a glass slide. Vale was the first to purify kinesin from the neurons of giant squids and to observe motor motility when the extract was placed on a glass slide with microtubules and other necessary chemicals [Vale, 1985, Cell]. Since then, a number of significant experiments have been done in vitro.

One important experiment performed by Selvin et al discerned between two models of kinesin's stepping: the 'inchworm' model and the 'hand-over-hand' model. In the inchworm model, the same head leads each step with the second head always following and coming to rest on the same tubulin subunit as the first head. In the hand-over-hand model (also described in the motor overview), the heads alternate taking the leading steps in the same way that bipeds like humans walk. Both models predict that the cargo's center of mass would move 8nm with each step, and because all current methods of measuring the step size measure the center of mass displacement, it has been impossible to determine which model is correct. Selvin's group took a different approach: they labeled one of the motor heads with a fluorophore and measured each displacement of that head. Given that the microtubule subunit separation is 8 nm and assuming that heads cannot share the same subunit, the inchworm model would predict that each motor head would move in steps of 8 nm with the center of mass of the cargo (the measured step size) moving the same distance per step. On the other hand, the hand-over-hand model would predict that each head would move 16 nm per step - the back head would skip over the front head in order

to bind in front of it, traversing a distance of 16 nm. The experimenters observed the fluorescent head moving 16 nm at a time, confirming that the hand-over-hand model was correct.

Many in vitro - and more recently, in vivo - experiments used a device called an optical trap or optical tweezers. In the simplest case, an optical trap consists of a visible or near-IR laser that is focused to a diffraction-limited spot on the sample in question. The theory underlying the optical tweezers will be discussed in depth later in this paper, but suffice it to say that the gradient of the laser's intensity generates a linear restoring force on a dielectric particle placed in the focus of the laser. Many molecular motor cargos, natural and artificial, can be trapped and therefore studied in such a trap. Once the trap's 'stiffness' is determined, the force applied to the particle can be determined. This has allowed investigators to measure the forces exerted by single motors (see table for measurements).

The same laser used to trap particles in an optical trap can also be used for high temporal- and spatial- resolution position detection with the use of a quadrant photodiode. This type of detection is well-suited to measuring the position of a cargo in time, and even the size(s) of individual steps of the molecular motors. This will also be described in more depth.

One of the most surprising in-vitro findings that made use of an optical trap was that dynein, but not kinesin, could alter the size of its steps in response to the force applied against it. That is, when a stronger force was applied to a walking dynein, it shortened its step size to 'downshift' [Gross, Nature, year?]. This is especially interesting because dynein alone possesses multiple ATP binding sites. Using a

variable number of ATP molecules could allow it to take differently-sized steps. The implications and importance of this will be discussed later.

In various model organisms, investigators have measured the properties of motion using Differential Interference Contrast (DIC) microscopy. A group under the direction of Wieschaus and Block [Wieschaus, 1998, Cell] identified a suitable system in Drosophila (fruit fly) embryos and recorded videos from DIC microcopy for analysis. Using image analysis software, they measured a few different parameters to characterize the motion: the amount of time that cargos traveled in a single direction before changing directions or stopping (persistence time), the average distance that a cargo traveled before changing direction or stopping, and the average velocity of the cargos in the plus- and minus-directions. They found that all of these parameters varied with the developmental stage of the embryo and concluded that cargo transport must be regulated tightly by the cell.

More recently, biophysicists have also found ways to use optical traps in vivo (in living organisms), and thus, have been able to study motors in their natural environments. Reliably determining the stiffness of an optical trap in vivo was the main challenge here. Now that this has become commonplace, however, the forces exerted by motors in vivo have been measured. See table for summary of results of these measurements.

One interesting experimental result found using the optical trap in vivo suggests that kinesin and dynein motors come in pairs or are otherwise tightly coupled together [Shubeita, Cell, year?]. This experiment was performed in Drosophila (fruit fly) embryos, an organism for which many mutant forms are available. The investiga-

Measurement	*kinesin*		*dynein*	
	in vitro	*in vivo*	*in vitro*	*in vivo*
Single motor force (pN)	7.2^{Block}	2.6^{george}	1.1^{ref}, 7^{ref}	1.1^{ref}, 2.4^{ref}, 3^{ref}
Step size (nm)	8^{Block}	8^{Sims}	8, 16, 24, 32^{gear}	?

Table 1: Various measurements of molecular motor parameters

tors used a fly genetic mutant that produces only approximately half of the number of kinesin motors that a normal fly does (the number of dynein motors was unaffected). Multiple motors can attach to a single cargo, so we would expect that each cargo in the described mutant would have fewer motors attached to each cargo on average. The average force can be thought of as the product of the average number of motors towing each cargo and the force exerted by a single motor. We would expect the average force exerted by teams of dynein to be the same as that measured in the non-mutant because the number of dyneins is unchanged compared to the mutant. We would expect the average force exerted by teams of kinesin, however, to be less than that measured in the non-mutant because the average number of kinesins attached to each cargo is less than in the non-mutant. When the scientists measured the average force for kinesin teams in this mutated type of fly, they found that it was decreased relative to the non-mutant, as expected. When they measured the average force of dynein teams in this type of mutated fly, however, they found that it was unexpectedly decreased by the same amount as kinesin. This result suggests that the dynein and kinesin somehow come as pairs.

1.4.3 The Future of Molecular Motors

A great deal has been learned about molecular motors over the past few decades, in large part thanks to biophysicists, but many important questions still need to be answered:

- What are the specific (at the atomic level) mechanisms of walking and force generation?
- What are all of the possible parameters of both motors' motion (step size, force generated, velocity, run length, etc.), and under what conditions are each realized?
- What determines what kind of cargo a molecular motor carries? Can parts of the motors be swapped in order to bind to different kinds of cargos? That there are many different types of kinesin but only one type of dynein suggests that there are different ways the motors recognize cargos.
- How do living cells regulate the direction of transport of their motors? At different time periods in the cell, distinct net transport occurs despite both kinesin and dynein being attached. What determines the net direction of that the cellular cargos travel? Two classes of models have been put forth, but neither has accrued conclusive experimental support:
  - Tug of war model: The net direction of transport is determined by which team of motors, dynein or kinesin, wins an effective tug-of-war. To regulate this, the cell could produce chemicals that change the binding, walk-

ing, or force generation properties in order to weaken one type of motor relative to the other to bias the random walk [6].

– Regulation model: The net direction of transport is determined by a chemical switch that unbinds one type of motor from the microtubule or prevents it from binding in the first place. As a consequence, the opposing motors never 'fight'.

2 My Work

2.1 Introduction

My work has focused on measuring the step size of the molecular motor, dynein. The step size is one of the most basic parameters of a molecular motor's motion. Dynein is especially interesting when one considers that, in vitro, it has been shown to change its step size in response to an applied force and that it has multiple ATP binding sites. Its ability to change its step size may be intricately tied to its regulation, and thus, the regulation of transport in the cell.

The step size of dynein has proved notoriously difficult to measure both in vivo and in vitro. No research group has confidently measured it in vivo, and amongst those that have measured it in vitro there is not consensus. One of the most significant factors that makes measuring the step size of a motor difficult is positional noise. Nearly all types of measurements of a motor's position actually measure the position of the motor's cargo, not the position of the motor itself. In other words, you infer the position of the motor from that of the cargo. This noise originates

from the fact that the cargo can experience constrained diffusion at the end of the motor it is attached to. The motor is not rigidly held erect; it can 'flop around'. Thus, even when the motor itself is at rest, the cargo can explore a significant region of space. Knowing the approximate length of the motor and the size of the cargo, we can estimate the maximum distance that a cargo could travel when attached to a stationary motor (figure 5). When making gross measurements of the motor (velocity, run length), the errors associated with this inference are negligible, but when measuring displacements as small as a few nanometers this noise becomes very important.

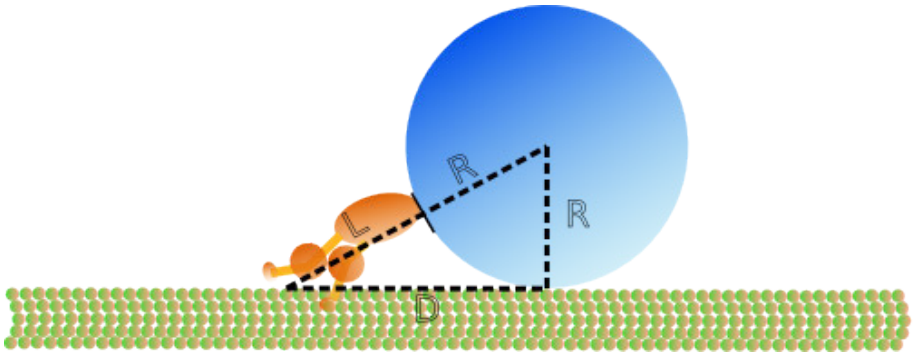

Figure 5: Schematic showing maximum cargo displacement due to positional noise

$$D = (L + R)\cos(\sin^{-1}(\frac{R}{L+R})) \approx 250\text{nm}$$

using $L = 100$ nm and $R = 250$ nm.

Nearly all previous attempts to measure its step size have made use of an optical trap. Because the trap exerts a restoring force on the cargo, the cargo does not diffuse nearly as much as it would if it were free of the trap. This way, the position of the

cargo is a more reliable approximation of the position of the motor. Because you are measuring the step size while applying a force to the motor, you are not measuring the step size in the motor's natural state. This becomes a significant consideration in light of the discovery that dynein can change its step size in response to applied force; applying a force to better measure the step size may, in fact, change the step size.

I attempted to measure the step size of dynein in vivo without the aid of an optical trap by recording videos of motor transport using DIC microscopy, tracking the movement of the cargo-motor complexes using a computer program, and computing a statistical distribution with the tracking program's output. The step size measured in this way would be independent of an artificial force, and thus, representative of dynein's actual function in vivo.

2.2 Background, Description of Experiment

2.2.1 Differential Interference Contrast (DIC) Microscopy

Differential Interference Contrast (DIC) microscopy is a powerful type of light microscopy available and one commonly used to study biological systems. As its name suggests, it relies upon interference due to the different relative phases of two electromagnetic waves to produce contrast. Neither image sensors nor the human eye can detect differences in the phase of light - they can only detect differences in intensity - so DIC microscopy produces visible contrast as follows:

1. Unpolarized light of a uniform wavelength is first passed through a linearly polarizing filter at 45 degrees.

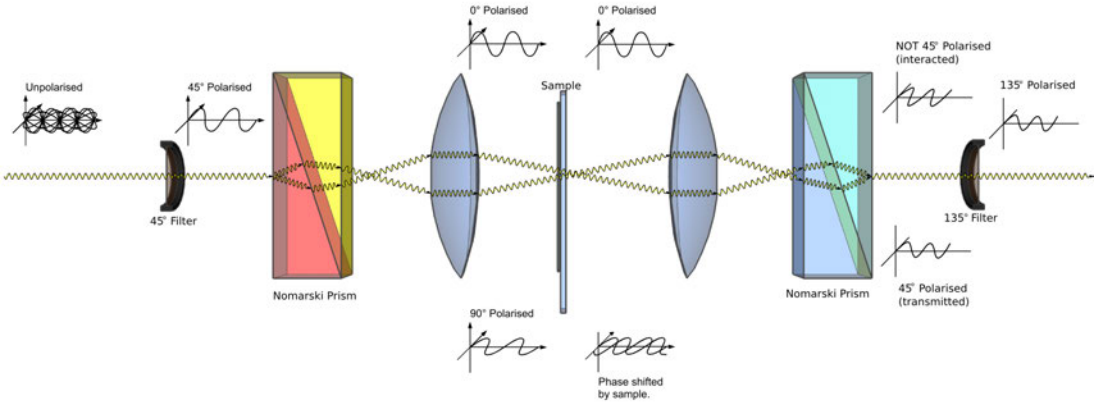

Figure 6: Schematic of light paths in Differential Interference Microscopy. Image modified from wikimedia foundation

2. This light then enters a special type of prism, called a Nomarski prism - that separates the 45 degree polarized light into two perpendicular components: one polarized at 90 degrees and one polarized at 0 degrees. This prism also spatially separates these two beams.

3. The condenser lens of the microscope focuses both beams in the sample plane where they interact with the sample. When one of the beams passes through an object with a different index of refraction (optical density), its phase is shifted relative to its sister beam.

4. Both beams are collected by the objective lens, and remain spatially separated until they are passed through another Nomarski prism.

5. The second Nomarski prism now recombines the two beams at which point they interfere destructively due to an acquired phase difference. Another way of thinking about this is that now, because one of the beam's phase was shifted

relative to the other, the resultant beam is no longer linearly polarized; it is elliptically polarized.

6. The resultant beam is then polarized at 135 degrees. Transmitted light that did not interact with the sample - that which still has a polarization of 45 degrees - will not pass through this filter. Light that interacted with the sample - that which has elliptical character - will have some component that passes through the 135 degree filter. An image sensor or human eye will be able to detect this component (figure 6).

Most types of visible light microscopy rely upon differences in index of refraction to produce contrast, but DIC is much more sensitive to these differences and, thus, can produce better images. In non-DIC visible light microscopy, contrast originates only from incident light being reflected from interfaces of two materials with different indices of refraction. I.e., the transmitted light does not contain any additional information. In DIC microscopy, however, the transmitted light carries information in its phase about the indices of refraction of the materials it passes through.

The best resolution that can be achieved with DIC is given by the diffraction limit, .5lambda., because the two split beams can only be focused within one-half of a wavelength of each other before they become indistinguishable. Green light of wavelength 530 nanometers was used in my experiment, meaning that objects within 265 nanometers of each other could only be seen as a single entity.

It is important to note that the diffraction limit does not prevent us from visualizing or tracking a particle smaller than the distance given by .5lambda; it only prevents us from distinguishing between two objects that are closer than .5lambda.

Using DIC to measure lengths smaller than 265 nanometers (.5lambda) does not, therefore, pose a theoretical concern.

2.2.2 Video Capture

To analyze the motion seen under DIC, video footage was recorded. The small time and distance scales probed in this experiment placed significant requirements on the camera.

First, the camera must capture enough frames per second to successfully measure individual steps. Based upon measurements of the in vivo velocity of dynein and its minimum step size, I estimated the maximum processivity (stepping rate) to be approximately 80 steps per second. To be certain that I am measuring steps, I require that I measure at least three frames per step. Thus, I require that the camera be able to capture approximately 250 frames per second.

The smallest fundamental brightness unit of a digital camera is a pixel. The pixel size of a camera determines the minimum separation between two distinguishable objects. Similar to the diffraction limit, though, the 'pixel limit' is not absolute; we are not prevented from probing smaller distances than a pixel in some cases. This is because pixels have more than one level of brightness (more than a single bit), and because the edges of the pixels are 'hard edges' - there is no overlap between adjacent pixels and no space in between. Theoretically, an upper bound of the minimum resolvable distance under ideal conditions is the length of the pixel / # of bits. Proof: Consider the figure (7) below; a square pixel of side length L and an object which illuminates the pixel whose projection onto the pixel entirely fills the

pixel but no more and also has 'hard edges'. Assuming that the illuminating object can take advantage of the entire dynamic range of the pixel, the pixel will measure maximal brightness when the projection of the object fully overlaps the pixel and minimal brightness when the projection does not overlap at all. As the projection of the object traverses the pixel from maximum coverage to zero coverage, the pixel will measure all values of brightness between its maximum and its minimum. And if the brightness that the pixel measures is linearly proportional to the intensity of the illuminating light, the distance that the object's projection travels between each decrease in brightness (in bits) of the pixel will be equally spaced, meaning that for each L ÷ #bits, the brightness will decrease by one bit.

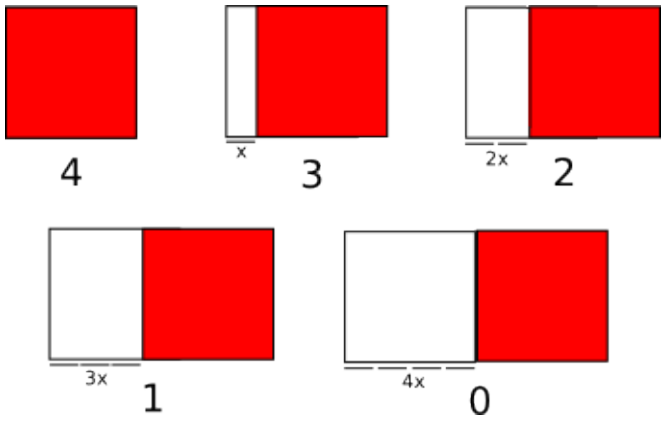

Figure 7: Schematic demonstration of one way to achieve sub-pixel resolution. The white square is the pixel; the red square is the image projection. The large number under each image is the 'brightness bit', and x = the side length ÷ # of bits. As the red square slides off of the pixel, the brightness will decrease by one bit for each unit of x, effectively measuring a distance smaller than the size of the pixel.

This goes to show that sub-pixel resolution is possible. Small pixel size is still a very important criterion, however, and was taken into account when choosing a camera.

The camera initially used for video capture was a Basler Scout, capable of (check maximum fps) frames per second, and whose pixels were (check pixel size).

2.2.3 Model System

I used Drosophila melanogaster (common fruit fly) embryos to study molecular motor transport. Drosophila offers a number of advantages. First, they are simple to culture, and the regeneration time and lifetime of Drosophila are very short, meaning that experiments can be conducted rapidly. More importantly, however, Drosophila is a very well characterized organism in terms of development, physiology, and genetics. Many strains of Drosophila are also available that possess genetic mutations that affect motor transport, opening the door to further experiments that might shed light on their function.

I conducted my experiments in Drosophila during a specific phase of development of the embryo called Stage 5. During this stage, biologists have determined that molecular motors vigorously transport a type of cargo called the lipid droplet near the periphery of the cell [Wieschaus, Cell]. Lipids are molecules that constitute the outer membrane of cells, and lipid droplets are merely spherical globules of lipids. On average, they measure approximately 500 nanometers in diameter. They are visible under DIC microscopy, making them viable cargos to study (figure 8).

2.2.4 Tracking Program

A computer program written in the National Instruments LabView environment was used to track (quantify) lipid droplet transport video-recorded under DIC microscopy

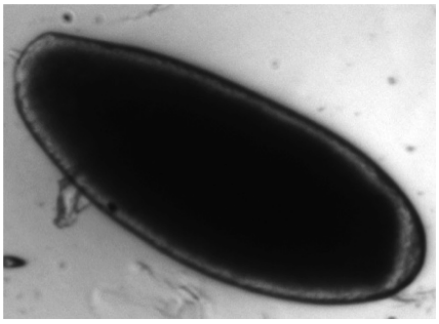

(a) Developmental stage prior to stage 5. Periphery of embryo is cloudy

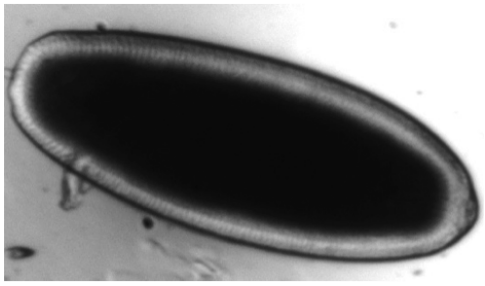

(b) Developmental stage 5. Molecular motors are responsible for clearing of lipid droplets near periphery

Figure 8

[reference for the person that wrote it in the Gross lab].

To use this program, a user imports a video file and selects a cargo to track by defining the smallest box that includes all the entire cargo. The user then defines a slightly larger box. The program's tracking algorithm searches for the image of the cargo defined by the first box in frame x within the image defined by the larger box in frame x + 1 by performing a mathematical operation called a cross-correlation using the intensity values of each pixel. The program determines the cargo's position in frame x + 1 as the maximum value of the cross-correlation.

After determining the position of the cargo in each frame of the video, a linear least-squares best fit of these positions is performed. The positions of the cargo in each frame are then projected onto this line, and these values constitute the output of the program. The line that these values are projected onto is intended to approximate the position of the microtubule on which the cargo-motor complex is walking. The microtubule's location is needed because we are interested in ultimately measuring the distance that the motor-cargo complex has moved along its microtubule;

the direction of walking is rarely aligned exactly with the x- or y-axis. I modified this program to allow the user to define the location of the microtubule for use in circumstances in which the linear fit is not desirable.

2.2.5 Pairwise Distribution

In a perfect world, the distance traveled by the cargo as a function of time would look like a step function, where the size of the 'steps' would correspond to the size of the steps taken by the molecular motor. Due to the positional noise of the cargo, however, the distance vs. time plot is much noisier than a step function and extracting the step size is much more difficult. To address this, I wrote a LabView program to compute the pairwise distribution using the distance vs. time data of a track to average out the noise and better visualize trends in the data.

In essence, calculating the pairwise distribution involves taking the difference in position between the first (time, distance) point (call it A) and the point one time-step after it (call it B) and saving this number. Next, the difference in position between the same (time, distance) point (A) and the point two time-steps after it (C) is taken and saved. This is repeated for the pairs AD, AE, and so on for every possible pair involving point A. Then, the same operation is performed with point B: BC, BD, and so on for the rest of the pairs involving point B without repeating AB. Eventually the difference in position between every two pairs of points in the data set is taken and saved.

A histogram of these computed differences is then plotted. If the track of the motor-cargo' complex's motion was a perfect step function (not realistic), this com-

putation would only yield values of the step size of the motor and multiples of the step size of the motor. The corresponding histogram would show Dirac delta-function peaks at these locations in the histogram (figure 9). The same computation performed on a realistic (noisy) data set would yield values both less and greater than, but close to, the step size of the motor. Its corresponding histogram would approximately show Gaussian curves whose peaks would be located at the step size of the motor as well as multiples of the step size. In other words, the noise of the data set leads to these peaks having some finite width. The peaks would become narrower as the data became less noisy or as many tracks were included in a single computation.

Mathematically, the collection of data constituting the pairwise distribution is calculated as:

$$\sum_{i=1}^{N} \sum_{j>i}^{N} (d_j - d_i)$$

Where d_i is the displacement of the ith point.

2.3 Protocol

2.3.1 Sample Preparation

Drosophila embryos were harvested from the agar coated lid of a fly-growing cup approximately two and one-half hours after being laid. Phase 5, the desired developmental stage, occurs two hours after laying on average. Embryos were observed under a low-magnification microscope for more definite signs of phase 5, and at

Figure 9

(a) Idealized distance vs. time plot

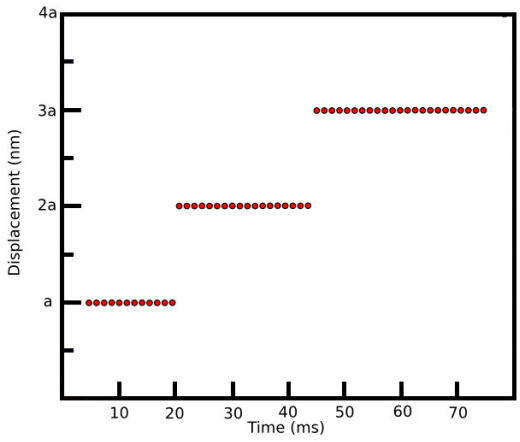

(b) Corresponding histograpm

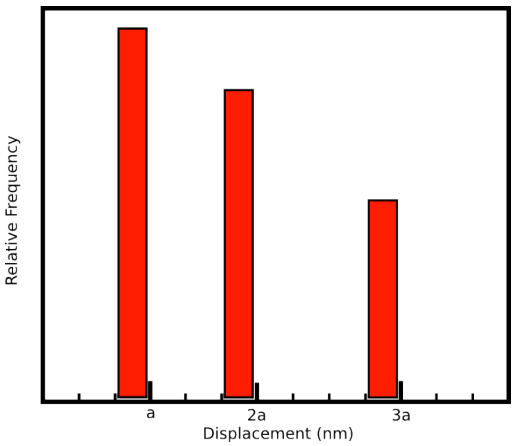

(c) Realistic (noisy) distance vs. time plot

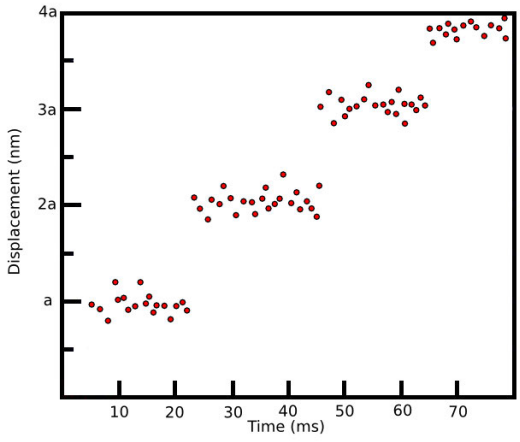

(d) Corresponding histogram

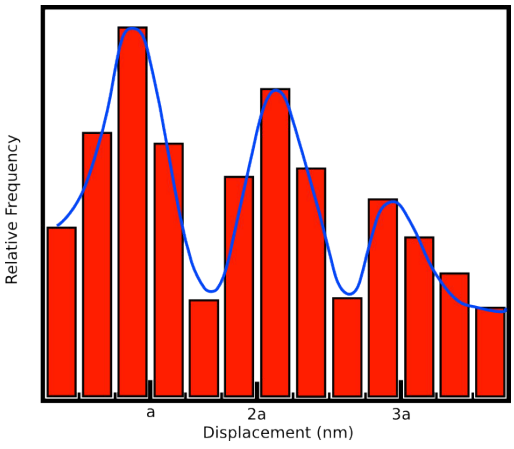

that point were prepared for the DIC microscope. Each embryo's chorion (tough, semi-transparent outer membrane) was peeled off with a precision tweezers to allow better transmission of light. The naked embryo was then placed on a glass slide with a notch slightly smaller in width and depth than the embryo itself, and a few drops of halocarbon oil were added. A thin glass coverslip was then placed on top of the other glass slide to flatten the embryo without rupturing it (figure 10). The best resolution is achieved with DIC when the sample is as thin as possible.

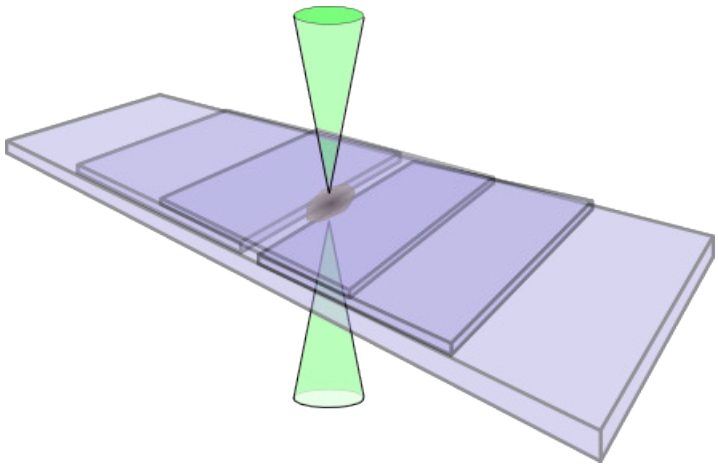

Figure 10:
Drosophila embryo]'Squashed' *Drosophila* embryo inside of glass slide. Green cone represents DIC light

2.3.2 Microscopy

The prepared sample was then moved to the DIC microscope. The microscope was focused near the periphery of the embryo where the transport occurs during phase 5. Because the orientation of the plus- and minus-ends of the microtubules in the embryo is known, one can identify the motors responsible for any observed transport

according to its direction. Any motion directed towards the periphery of the embryo is minus-end directed (dynein), and any inward motion is plus-end directed (kinesin) [21].

Upon identifying periods of vigorous transport, segments of video footage were recorded, taking note of the location of the periphery and center of the embryo.

2.3.3 Tracking

Lipid droplets were selected for tracking on the bases of: a) exhibiting relatively long periods of movement in a single direction, and b) not impacting other lipid droplets or objects that would hinder motion.

2.3.4 Analysis

After tracking, the plots generated from each track were analyzed by computing the pairwise distribution.

2.3.5 Results and Discussion

By eye, it was clear from the plots generated by the tracking program that this method of measuring the step size would not produce results - not even rough steps were visible. Computation of the pairwise distribution confirmed that steps were not present.

This method may have failed to produce results for a few reasons. Most likely, the positional noise due to diffusion masked the steps of the motor.

Another complicating factor is that multiple dynein motors can attach to the

same cargo. If, for example, two dyneins were attached a single cargo and only one of them took a step, the cargo would only move half the distance it would have moved if only one motor were attached. Even more complicated apparent step sizes are possible when more than two motors are present.

It is also possible that my estimated minimum framerate for the camera was too low and that the camera did not capture enough frames per step of the motor.

2.4 Back to the drawing board

2.4.1 Background

To address the potential concerns of the original experiment, multiple modifications were made to the setup and protocol.

In order to reduce the thermal motion of the cargo and to reduce the processivity rate of the motor to increase the frames captured per step, a graduate student and I designed and built a new microscope stage cooled by Peltier elements. Peltier elements are solid state devices that make use of the Peltier effect, the tendency of heat to flow across a junction of two different metals when a current also flows across that junction. This effect is similar in spirit to the Joule-Thomson effect. One important consideration of cooling was that the embryo could not survive at temperatures lower than 18 C. This constrained how much cooling we could apply. The microscope room in which the experiments were conducted was also cooled to 18 C.

To reduce the average number of dynein attached to each cargo, I used a genetically mutated strain of Drosophila (KHC-27) which produced only half the normal

Figure 11

(a) Peltier stage (right) and controller (left)

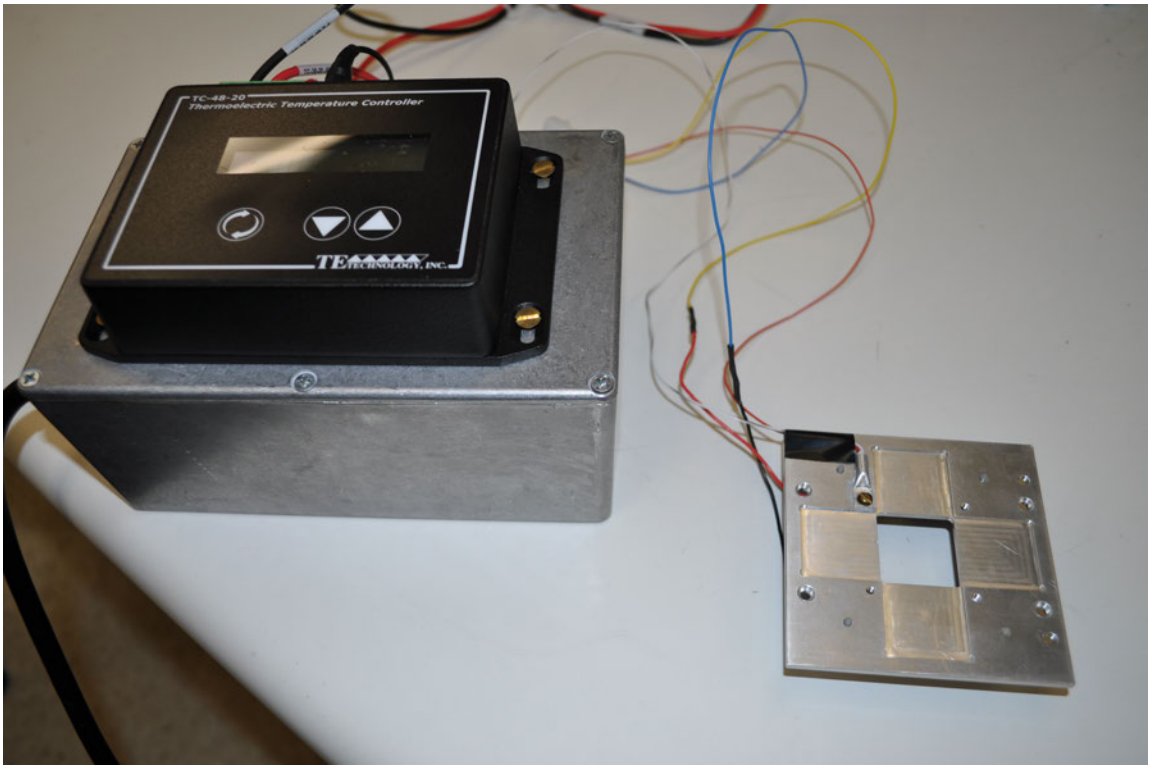

(b) Bottom side of stage, Peltier elements visible

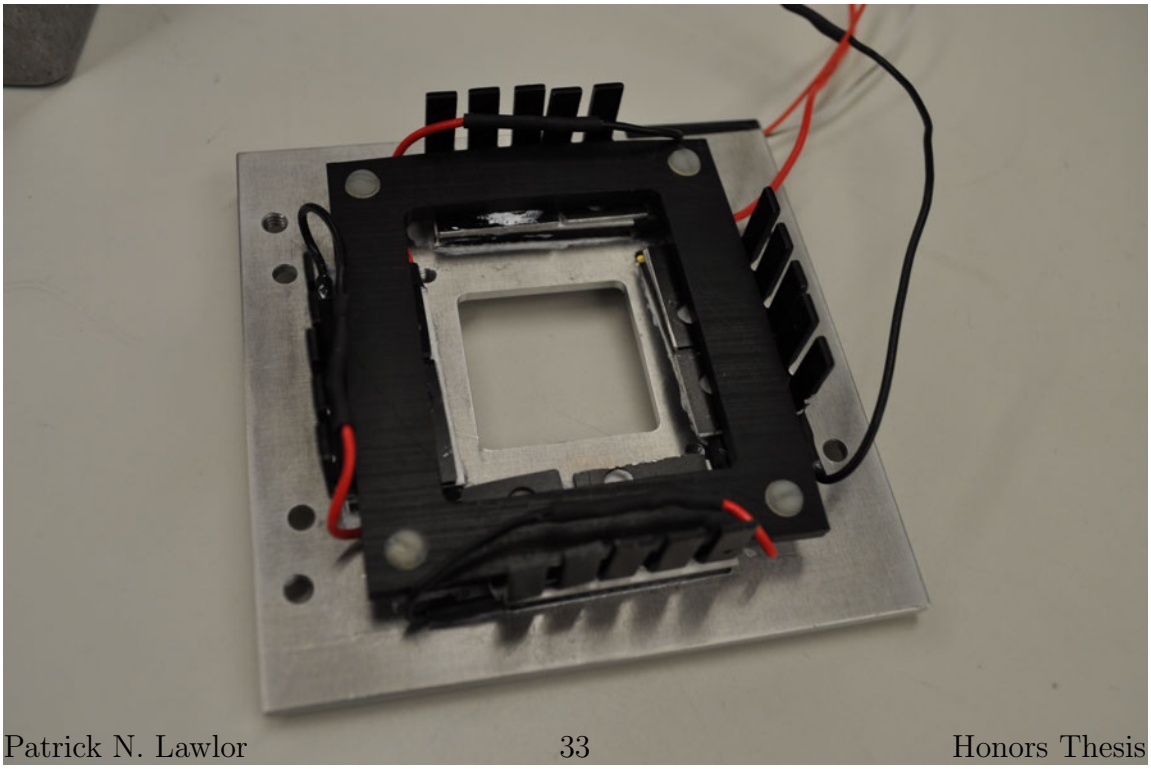

number of kinesin motors. On the basis of Shubeita el al's finding that dynein and kinesin motors come in pairs, it is relatively safe to assume that the number of dyneins attached to a given cargo was reduced by the same amount as kinesin.

I also experimented with a number of different types and brands of digital cameras in order to find one that could capture more than 250 frames per second and was sensitive enough to produce video that could still be reliably tracked. I eventually selected the Basler Aviator.

2.5 Protocol

Same as In Vivo I.

2.6 Results and Discussion

Even with modifications made to the experiment to address the positional noise, multiple dynein motors per cargo, and insufficient frame rate, this experiment failed to yield a believable step size for dynein. See histogram calculated using the pairwise distribution.

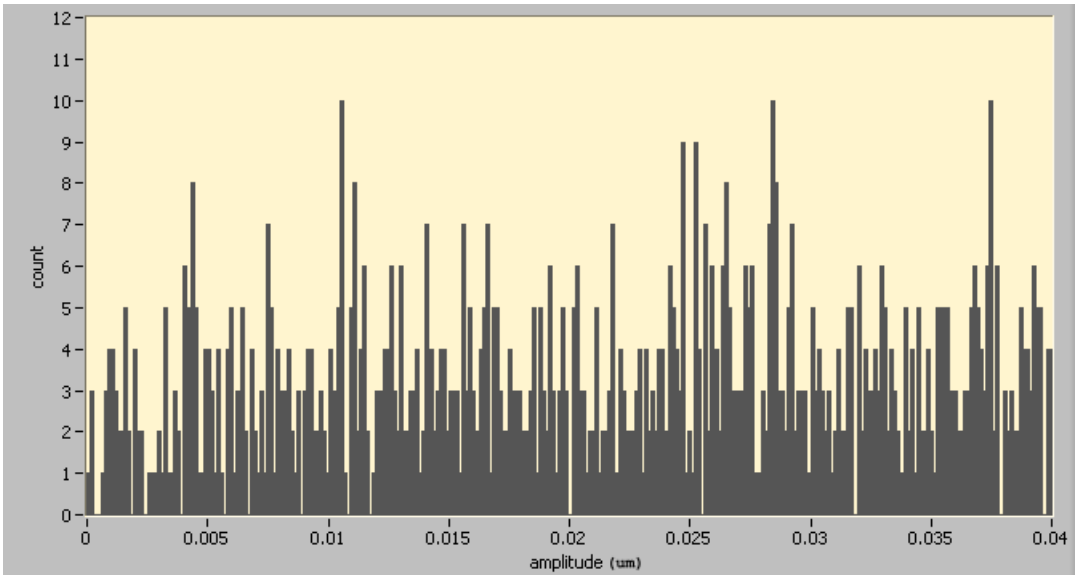

Figure 12: Histogram of a single track. No clear, consistent peaks visible

Peaks at integer-multiples of the step size - that we would expect to see if distinct steps were present - were not present. We can conclude, therefore, that there were not differences in displacement that were consistently measured.

It is most likely that the positional noise still masked the steps of the motor

despite efforts to reduce it. Even when the cargo does not seem to impact any objects in its surroundings, it is very possible that it does come into contact with proteins, vesicles, or other organelles that are not visible with DIC microscopy.

Another possibility is that slight heterogeneities in the cytosol prevent the cargo from moving smoothly enough to allow us to discern individual steps. These heterogeneities could arise from local chemical releases or chemical gradients that exist naturally in the cell.

3 Ex Vivo

Not having been able to measure the step size of dynein in vivo using DIC and video tracking, I began to collaborate with a graduate student to attempt to measure the step size of dynein in a different system that he is pioneering, ex vivo.

The ex vivo approach involves purifying the cargo-motor complexes from lysed (punctured) embryos using centrifugation, and quickly placing them in a sufficiently shallow channel on a glass slide along with microtubules and ATP. Because the motor-cargo complex has been recently purified from the living organism, the complex may contain bound protein or chemical signals that influence the step size or other aspects of motor behavior. These signals would not necessarily be included in the system if the motors were purified in another manner and stored for long periods of time before use (typical of in vitro experiments).

Because this type of experiment involves using components recently taken from a living organism and placed on a glass slide, it falls somewhere between in vivo and in vitro. Ex vivo is intended to produce more realistic results than in vitro experiments,

but without the complication and baggage of in vivo experiments. For example, ex vivo experiments can be prepared without unnecessary cytoplasmic constituents, the genetic control of the cell is removed, and the conditions can be held effectively static compared to those of the living organism. The results will be much easier to interpret because there are few unknown factors besides the chemicals bound to the purified complexes.

But instead of attempting to measure the step size of dynein using DIC and video tracking, I will use an optical trap. While Drosophila embryos are too thick and heterogeneous to allow for position detection using an optical trap, ex vivo samples are not. The optical trap will allow me to reduce the positional noise of the cargo and measure the position of the cargo at kilohertz rates.

3.1 Background

3.1.1 Optical Trapping

Optical trapping refers to the use of a focused laser to hold small dielectric particles in place. For particles much greater in size than the wavelength of light (the case at hand), the force that holds the particle in place results from the conservation of momentum.

Lasers have Gaussian profiles, meaning that the intensity of the laser is the greatest at its center and drops off like a Gaussian as you near the edge of the laser. When a laser is focused on a dielectric particle and the particle remains in the center of the focus, the same amount of light passes through the left side of the particle as passes through the right side. Because the dielectric particle has an index of refraction

greater than that of the particle's surroundings, the light refracts towards the center of the trap (figure 13). And because photons possess momentum, this refraction represents change in momentum. It just happens that the changes in momentum exactly cancel one another.

When, however, the particle moves out of the center of the laser, more light is passing through the side of the particle nearest the center of the laser because of the Gaussian profile. More light, then, is refracted from the inside of the particle towards the outside of the laser than vice versa, causing a net momentum change towards the outside of the laser. To conserve momentum, the dielectric particle must move towards the center of the laser until exactly the same amount of light passes through the left and right sides. Thus, a stable equilibrium point arises in the center of the laser. The force that results from this energy well is $F = .5\alpha * gradE^2$, proportional to the gradient of the electric field squared. For this force to be substantial, the change in magnitude of the electric field must occur over as small of a distance as possible. This is realized in the focus of the laser. Also of import is that the restoring force is linear over a wide range, allowing us to use Hooke's law when the stiffness of the trap is known.

The stiffness can be measured by allowing a dielectric bead of known size to experience constrained diffusion under the influence of the trap and while being recorded with DIC microscopy. The power spectrum of its motion can be calculated, and then fit to a Lorentz function which includes a constant that allows the determination of the stiffness of the trap.[16]

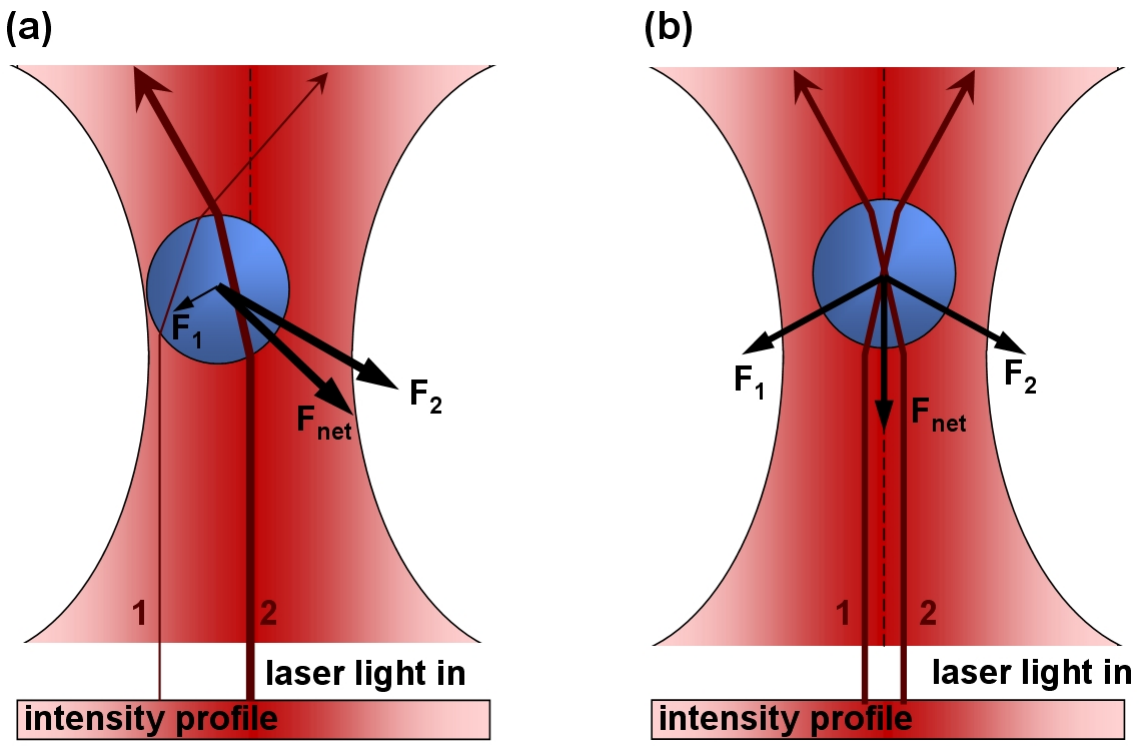

Figure 13: *(a)*: Particle at equilibrium in center of trap; amount of light refracted left and right exactly cancel. *(b)*: Particle displaced from equilibrium; more light refracted left than right; net force results to the right to conserve momentum. Figure from wikimedia foundation.

3.1.2 Position detection

The ability of the optical trap to generate a restoring force on a particle was its foreseen purpose, but the laser can also be used to determine the position of the trapped particle. When the laser is focused on a quadrant photodiode, the small deflections in its path caused by the movement of the particle can be detected as differences in intensity measured across the halves of the photodiode in the x- and y-directions. These differences in intensity are linearly proportional to the position of

particle over a certain range, allowing us to reconstruct the position of the particle. Theoretical treatment by Schmidt et al leads to the following functional form for the relative difference in intensity across two halves of the photodiode along a single axis.

$$\frac{I_+ - I_-}{I_+ + I_-} \approx \frac{16}{\sqrt{\pi}} \frac{k\alpha}{w_0^2} exp(-2(x/w_0)^2) \int_0^{x/w_0} exp(y^2)\, dy$$

where $k = \frac{2\pi}{\lambda}$ according to the laser's wavelength, w_0 is the e-folding distance of the narrowest part of the beam, and α is the susceptibility of the tracked particle. See figure 14 for graph of theoretical prediction and experimental data obtained by moving a silicon bead through the optical trap using a piezo motor stage in increments of 8 nanometers [5].

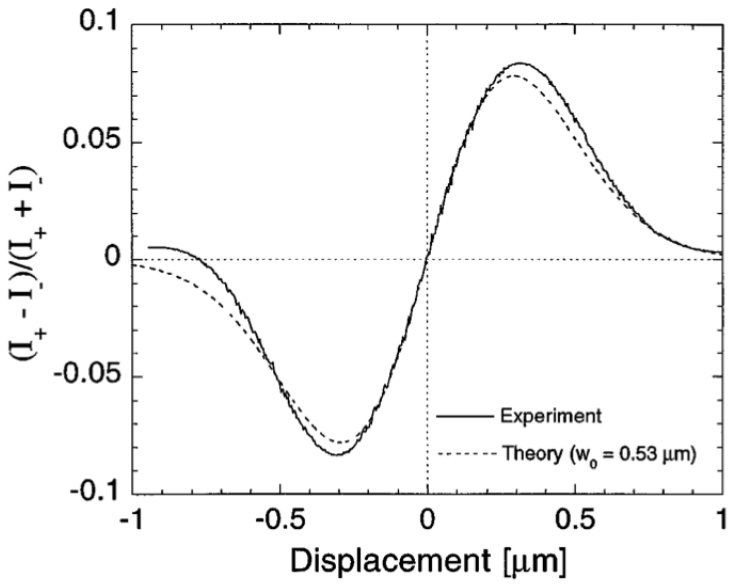

Figure 14: Theoretical prediction and experimental data for a dielectric sphere moving through an optical trap [5]

3.1.3 Microtubule Orientation

Because ex vivo experiments are carried out on a glass slide, microtubules are not present naturally; they must be added manually in order for the motors to walk upon. But while all of the microtubules are naturally oriented in the same direction in the Drosophila embryo, they are randomly oriented after being injected into the ex vivo sample chamber. The microtubules can be seen under DIC microscopy, but the plus ends are indistinguishable from the minus ends, meaning that motion due to kinesin cannot be distinguished form motion due to dynein.

To solve this problem, Mallik et al proposed a method to label the minus ends of microtubules that takes advantage of the biotin-avidin bond, the strongest biological non-covalent bond[11]. The essence of this method is:

1. First, polymerize microtubules with tubulin subunits that have the molecule biotin attached to them.

2. Next, break these long microtubules into smaller segments by passing them through a narrow needle

3. Extend the microtubule 'seeds' from the previous step by polymerizing them with a mixture of normal tubulin and NEM tubulin. NEM tubulin prevents polymerization from the minus end of the microtubule. The resultant microtubules will have segments at their minus ends built from biotin-labeled tubulin.

4. Beads visible under DIC that have had avidin molecules attached to them are combined with the microtubules. The biotin and avidin molecules will bind

very tightly, and the non-bound beads can be washed out. The minus-end segments containing biotin-labeled tubulin will now have visible beads bound to them, allowing identification of the minus ends under DIC.

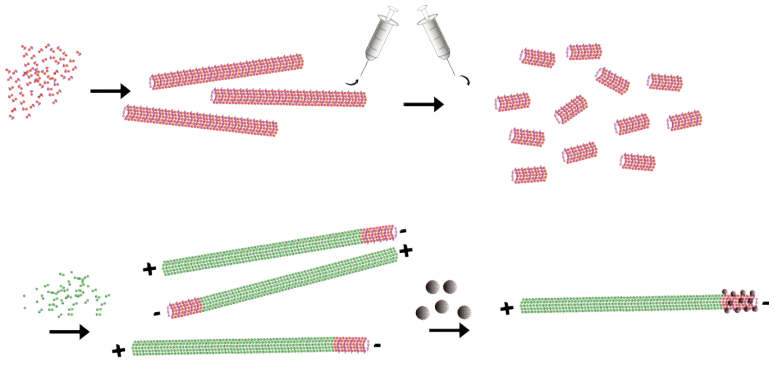

Figure 15: Microtubule minus-end labeling scheme

3.1.4 Results and Discussion

I have constructed the optical trap in a setup given by the schematic in figure 16. I have also assembled a quadrant photodiode device (figure 17) for use in particle detection.

Along with another undergraduate, I am currently working to implement the method for labeling the minus-ends of microtubules. While not complete, significant progress has been made to improve the affinity of the avidin-labeled beads for the biotin-labeled minus-ends, and to reduce the non-specific binding of beads to the glass slide. See Appendix A for detailed biochemical labeling protocol - specifics will not be discussed here.

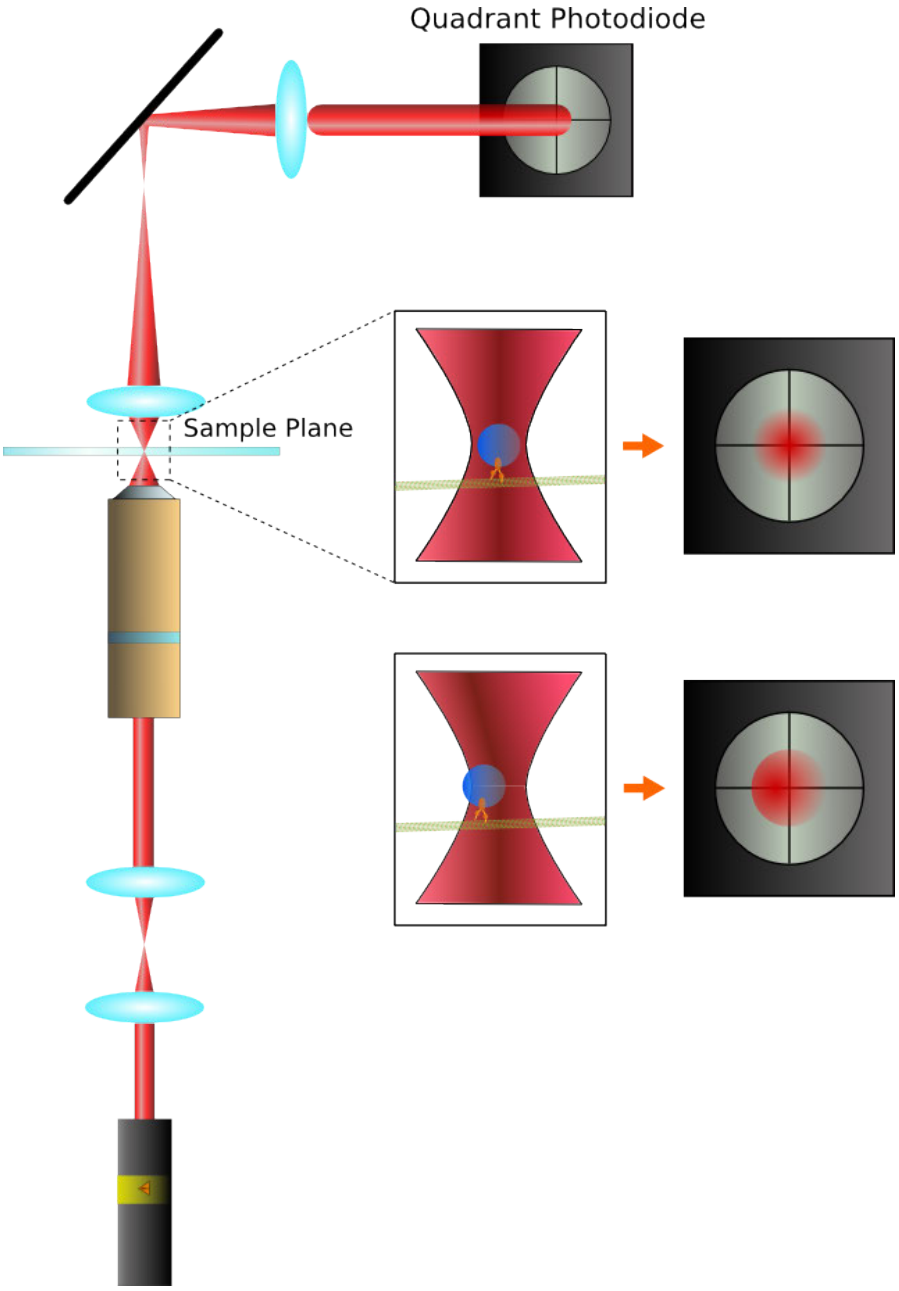

Figure 16: Schematic of optical trap setup with simplification of position detection mechanism using quadrant photodiode

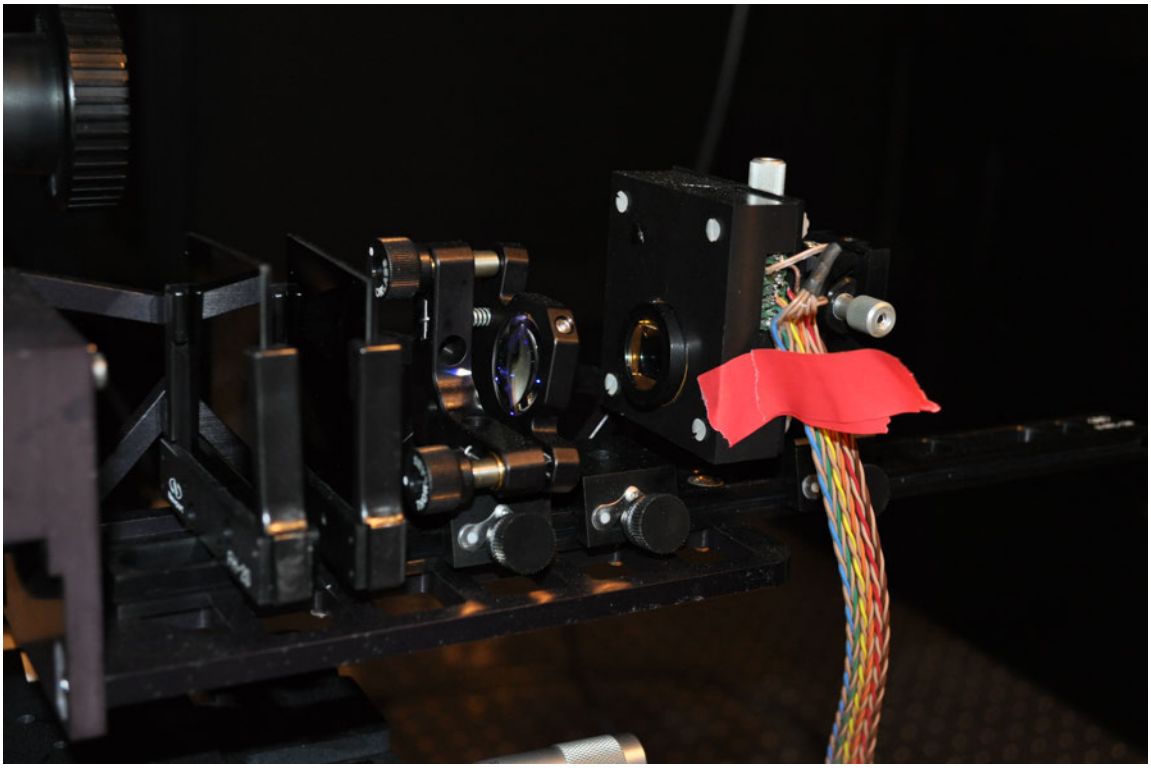

Figure 17: Photodiode apparatus. Black box on right contains amplifier card and photodiode itself (visible as circular aperture). Lens to the left of the photodiode focuses light on the sensor.

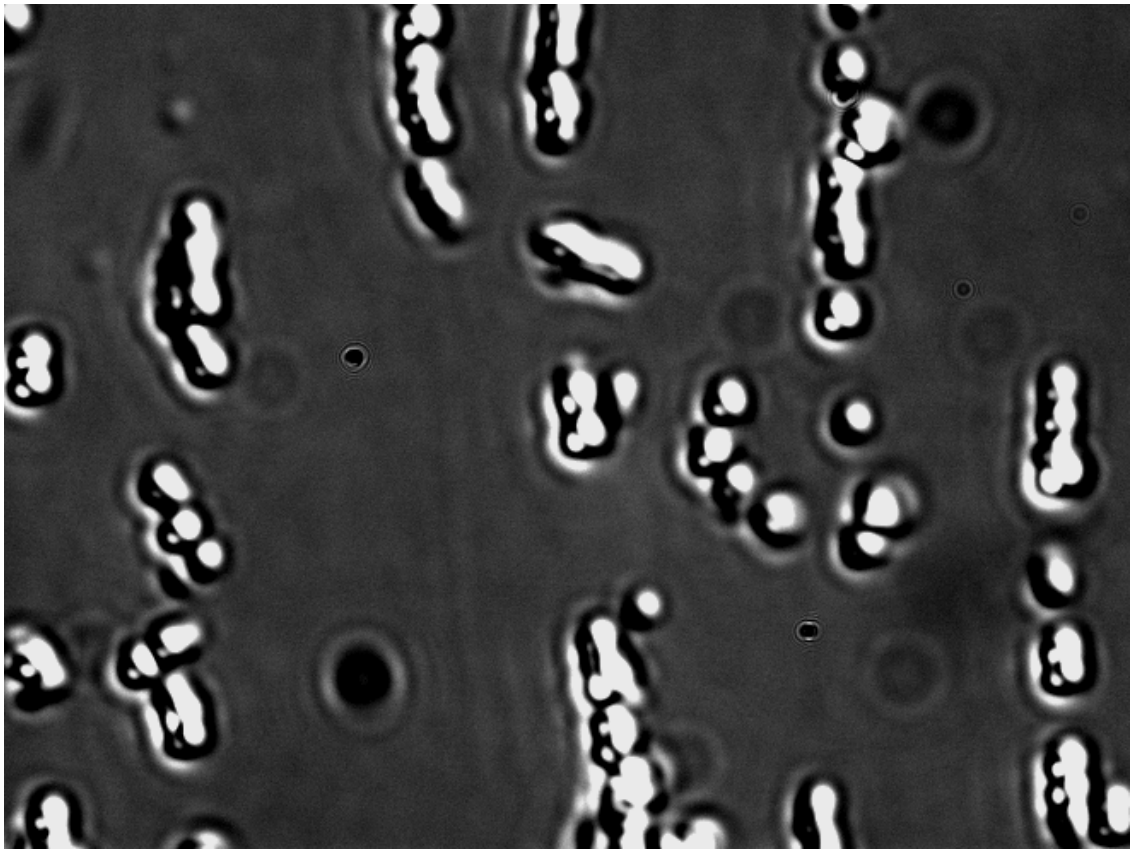

Figure 18: Initial labeling trial. Beads and microtubules visible (as faint lines). Bead concentration is far too high and large number of beads not bound to microtubules.

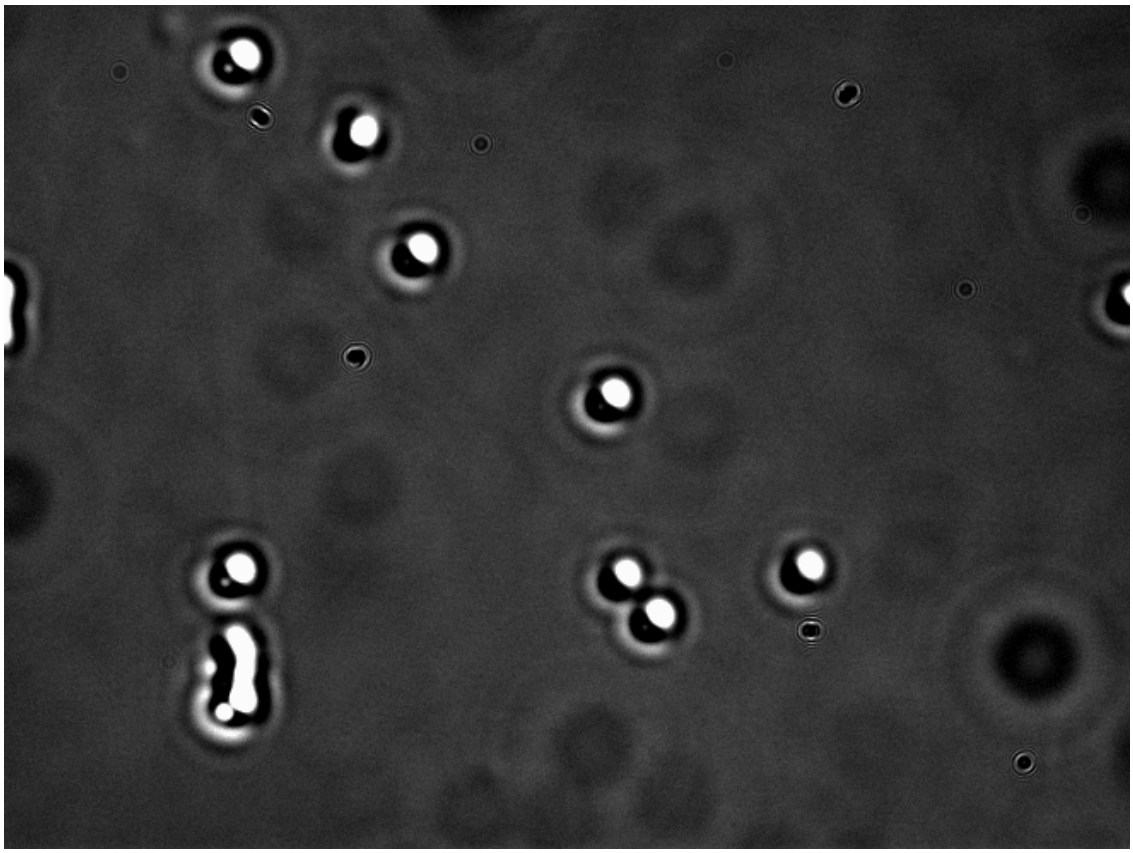

Figure 19: One major problem: non-specific binding of beads to glass surface.

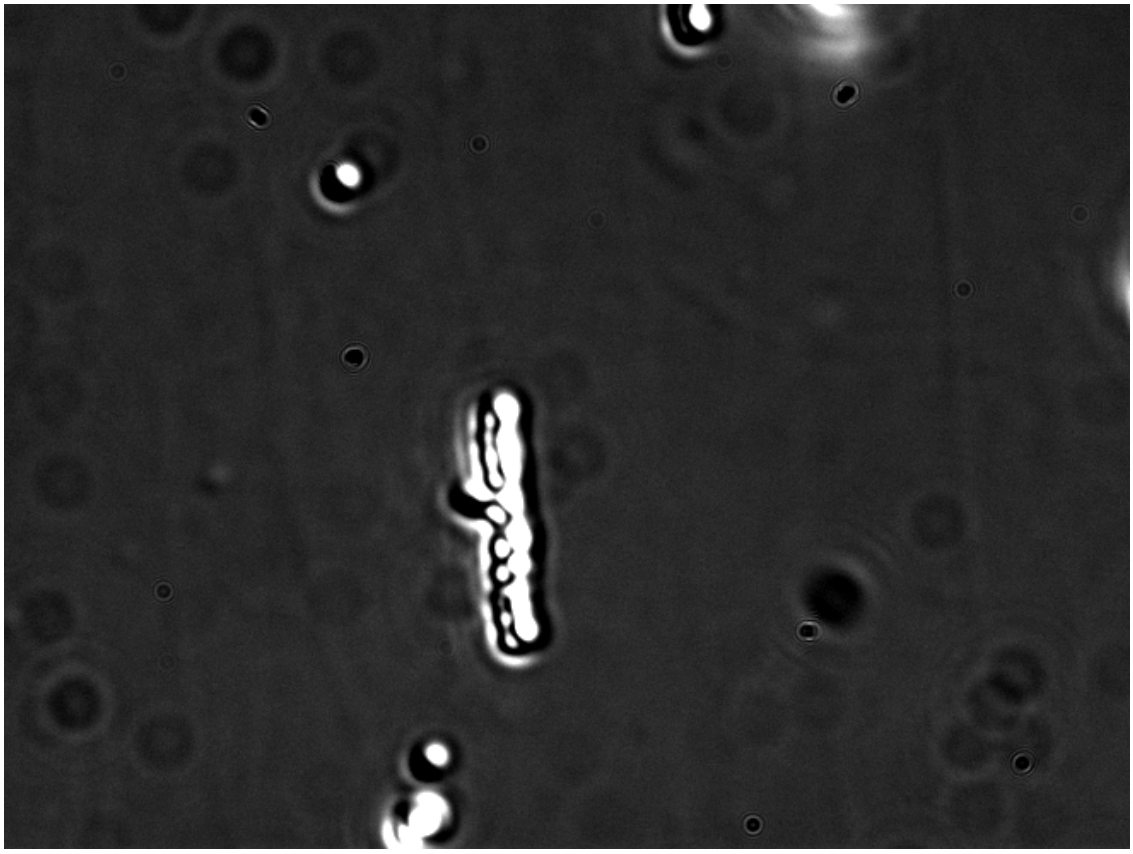

Figure 20: Advanced labeling trial. Labeled end of microtubule very clear, non-specific binding low.

4 References

1. Amos, L A. "Kinesin from pig brain studied by electron microscopy." JOURNAL OF CELL SCIENCE 87 (1987): 105-111. Print.

2. Block, Steven. "Kinesin Motor Mechanics: Binding, Stepping, Tracking, Gating, and Limping." Biophysical Journal 92 (2007): 2986-2995. Print.

3. Burgess, S. "Dynein structure and power stroke." Nature 421 (2003): 715-718. Print.

4. Carter, N J. "Mechanics of the kinesin step." Nature 435 (2005): 308-312. Print.

5. Gittes, Frederick, and Christoph Schmidt. "Interference model for back-focal-plane displacement detection in optical tweezers." Optics Letters 23.1 (1998): 7-9. Print.

6. Gross, Steven. "Coordination of opposite-polarity microtubule motors." Journal of Cell Biology 156 (2002): 715-724. Print.

7. Khalil, Ahmad. "Kinesin's cover-neck bundle folds forward to generate force." PNAS 105.49 (2008): 19247-19252. Print.

8. King, Stephen. "AAA domains and organization of the dynein motor unit." JOURNAL OF CELL SCIENCE 113 (2000): 2521-2526. Print.

9. Liu, Jun-Feng. "Crystal structure of human dynein light chain Dnlc2A: structural insights into the interaction with IC74." Biochemical and Biophysical Research Communications 349 (2006): 1125-1129. Print.

10. Mallik, Roop. "Cytoplasmic dynein functions as a gear in response to load." Nature 427 (2004): 649-652. Print.

11. Mallik, Roop. "Simple non-fluorescent polarity labeling of microtubules for molecular motor assays." Biotechniques 46 (2009): 543-549. Print.

12. Mitchison, Tim. "Role of GTP hydrolysis in microtubule dynamics: information from a slowly hydrolyzable analogue, GMPCPP." Molecular Biology of the Cell 3 (1992): 1155-1167. Print.

13. Numata, Naoki. "Molecular mechanism of force generation by dynein, a molecular motor belonging to the AAA+ family." Transactions of the Biochemical Society 2008 (2008): 132-135. Print.

14. Selvin, Paul. "Kinesin Walks Hand-Over-Hand." Science 404 (2004): 676-678. Print.

15. Shubeita, George. "Cargo transport: two motors are sometimes better than one." Current Biology 17 (2007): 478-486. Print.

16. Shubeita, George. "Consequences of Motor Copy Number on the Intracellular Transport of Kinesin-1-Driven Lipid Droplets." Cell 135 (2008): 1098-1107. Print.

17. Sims, Peter. "Probing Dynein and Kinesin Stepping with Mechanical Manipulation in a Living Cell." ChemPhysChem 10 (2009): 1511-1516. Print.

18. Vale, Ronald. "Identification of a novel force-generating protein, kinesin, involved in microtubule-based motility." Cell 42 (1985): 39-50. Print.

19. Vale, Ronald. "The way things move: looking under the hood of molecular motor proteins." Science 288 (2000): 88-95. Print.

20. Vale, Ronald. "The molecular motor toolbox for intracellular transport." Cell 112 (2003): 467-480. Print.

21. Wieschaus, Eric. "Developmental Regulation of Vesicle Transport in Drosophila Embryos: Forces and Kinetics." Cell 92 (1998): 547-557. Print.

22. Williams, John. "Crystal structure of dynein light chain TcTex-1." Journal of Biological Chemistry 280 (2005): 21981-21986. Print.

23. Williams, John. "Structural and thermodynamic characterization of a cytoplasmic dynein light chain-intermediate chain complex." PNAS 104 (2007): 10028-10033. Print.

24. Yildiz, Ahmet. "Kinesin walks hand-over-hand." Science 303 (2004): 676-678. Print.